Realizing controllable depolarization in photonic quantum-information channels

A. Shaham and H. S. Eisenberg

Racah Institute of Physics, Hebrew University of Jerusalem, Jerusalem IL-91904, Israel

Controlling the depolarization of light is a long-standing open problem. In recent years, many demonstrations have used the polarization of single photons to encode quantum information. The depolarization of these photons is equivalent to the decoherence of the quantum information they encode. We present schemes for building various depolarizing channels with controlled properties using birefringent crystals. Three such schemes are demonstrated, and their effects on single photons are shown by quantum process tomography to be in good agreement with a theoretical model.

I. INTRODUCTION

Light depolarization is a fundamental optical phenomena. It was studied as early as the nineteenth century, when measurement and characterization methods of the polarization state of light were introduced [1]. Methods for complete depolarization of light, such as the Cornu and Lyot depolarizers, have been known for many decades [2–4]. The Cornu and wedge depolarizers require the light beam to be wide, as the loss of coherence between the two polarizations is achieved via averaging over the spatial degrees of freedom. In the case of the Lyot depolarizer, short coherence length is required and the averaging is over the temporal degrees of freedom. Nevertheless, there are currently no methods that enable control of all of the aspects of the depolarization process.

Quantum information is commonly encoded in the polarization of single photons [5]. Depolarization of such photons acts as quantum noise on the stored information; that is, the interaction between the information encoding units and the environment results in decoherence. In order to study quantum decoherence in general and its effect on quantum information protocols in particular, it is desirable to create quantum channels with controlled noise. Such channels will be useful for testing quantum error correction and quantum key distribution protocols [6,7]. Controlling the noise properties of a channel enables the study of the information transfer rate in the presence of different noise types, with different symmetries. One can also compare between suggested communication schemes by testing their performance and their robustness with respect to channel noise properties. Other uses for these channels are to test for the existence of decoherence-free subspaces [8] and for generating partially mixed entangled states [9].

In recent years, depolarizing channels were studied by several methods. When a single birefringent crystal was used, only dephasing channels were demonstrated, as we show later [8]. Optical scatterers such as emulsions, multimode fibers, and ground glass give variable depolarization but are also accompanied by a spread in k space, resulting in considerable loss when collected for further processing [9–11]. Another approach is to use polarization scramblers of various kinds [12,13]. These realizations are equivalent to fast polarization rotations and averaging measurements over times longer than the typical rotation periods. Nevertheless, when used with single photons, each photon by itself is completely polarized.

Controllable depolarizers were demonstrated by using two wedge depolarizers with variable beam diameter [14] or a tunable relative angle [15]. These channels are hard to model, and their anisotropy level is uncontrolled as they couple the polarization with many spatial degrees of freedom.

In this paper, we present a theoretical and experimental study of various controllable depolarizing channels. We study channels that are composed of a sequence of birefringent crystals and wave plates. The depolarization and its anisotropy depend on the order and relative angles between the channel components. The generated channels are mostly anisotropic and can be tuned continuously between no depolarization and complete dephasing. These channels were characterized by the transmission of polarized single photons, generated by spontaneous parametric down-conversion. Quantum process tomography (QPT) was used to compare the experimental results with theory [16,17].

II. THE MODEL

The information in a classical channel can be degraded only by bit-flip errors. Thus, such a channel is completely described by a single parameter—the bit-flip error probability. In comparison, quantum channels can have a constant unitary rotation and three types of errors, represented by the Pauli operators: a bit-flip that swaps the logical $|0\rangle$ and $|1\rangle$ amplitudes, a phase flip between the amplitudes, and the combination of the two, which is a third orthogonal operation. Isotropic decoherence is the case when the three error probabilities are equal.

A polarization qubit can be described either by a density matrix operator $\hat{\rho}$ or equivalently by a point in the Poincaré sphere. The Cartesian coordinates of this point are the Stokes parameters $\overline{S} = \{S_1, S_2, S_3\}$, which describe the linear horizontal and vertical ($|h\rangle, |v\rangle$), linear plus and minus 45° ($|p\rangle = (|h\rangle + |v\rangle)/\sqrt{2}$, $|m\rangle = (-|h\rangle + |v\rangle)/\sqrt{2}$), and right and left circular ($|r\rangle = (|h\rangle + i|v\rangle)/\sqrt{2}$, $|l\rangle = (i|h\rangle + |v\rangle)/\sqrt{2}$) polarization components, respectively. The degree of polarization (DOP) is defined as D, the length of the Stokes vector [18]:

$$D = \sqrt{S_1^2 + S_2^2 + S_3^2} \equiv \sqrt{1 - 4det(\hat{\rho})}. \qquad (1)$$

The perfectly polarized states are described by the surface of the sphere ($D = 1$), and its center designates the completely unpolarized state ($D = 0$). The inside of the sphere includes all partially polarized states ($0 < D < 1$). The physical meaning

of the DOP is the ratio between the polarized light intensity and the total light intensity. Therefore, an optical polarization communication channel that reduces the DOP to η has an information error rate of $\frac{1-\eta}{2}$.

Consider an arbitrarily polarized wave packet that is passing through a birefringent crystal [19]. The temporal walk-off $\tau = L\frac{\Delta n}{c}$ between two wave packets, each polarized along one of the symmetry axes of the crystal, depends on the crystal length L, its refractive index difference Δn, and the speed of light c. We assume that the coherence time of the wave packets t_c is shorter than the walk-off τ. If the light wave packet is not polarized linearly along one of the crystal symmetry axes, its two components acquire temporal distinguishability. Thus, the polarization and temporal degrees of freedom become entangled. The role of the environment in general decoherence models is fulfilled here by the temporal degrees of freedom. As the detectors are insensitive to the short temporal walk-offs, they cannot distinguish between the wave packets, effectively tracing out the temporal degrees of freedom. The result is an effective depolarization since no coherence can be observed between the two orthogonal polarizations. The depolarization operation is described in the Poincaré sphere picture by a projection of the initial Stokes vector on the direction that represents the crystal principal axes. For example, a birefringent crystal aligned along the h-v directions will project any initial state onto the S_1 direction. This kind of operation is referred to as a *dephasing channel* [5].

A single-crystal configuration can apply any level of depolarization to any initial linear polarization. On the other hand, for such a configuration there is always another polarization direction that experiences no depolarization whatsoever. Thus, we consider a second crystal that is placed after the first one [4]. For historical reasons, let us first assume that the second crystal is twice as long as the first one. The two crystals are coupling orthogonal temporal degrees of freedom, as the first crystal couples $t = 0$ with τ, while the second couples $t = 0$ with 2τ and $t = \tau$ with 3τ. Thus, this configuration can be described as two consecutive projections of the initial polarization state onto the Stokes directions defined by the crystals' axes. In the case where the orientation of the crystals differ by $45°$, the two projections are perpendicular, resulting in a final state at the sphere center ($D = 0$, the completely unpolarized state) for any initial state. This configuration in known as the *Lyot depolarizer* [3,4].

The relevant error rates for practical tests of quantum information protocols are less than 20%. For example, the six-basis quantum key distribution protocol with qubits has a recent upper limit of 14.59% for the error rate [20]. For this reason, it is desirable to have a depolarizing scheme that can be tuned to small values of depolarization or even to zero depolarization. Thus, we investigate a configuration of two identical crystals. If the second crystal is oriented at $90°$ with respect to the first one, the polarization time delay created by the first crystal is exactly compensated for by the second. For any other relative angle, there can be up to three different temporal modes: $t = 0$ and τ are coupled by the first crystal, while the second crystal couples between them and an additional third delay $t = 2\tau$. Changing the relative angle between the two crystals affects the occupation of each of the

three modes, which results in a different depolarization. Hence, by tuning this angle we control the channel depolarization level.

The final polarization state can be easily calculated for a given initial polarization and tuning angle, using the density operator formalism of the decoherence process [16]: We denote the initial polarization state with the two-dimensional density matrix $\hat{\rho}$, and the environmental degrees of freedom with the density matrix $\hat{\rho}_{\text{env}}$. After an interaction $\hat{U}$ between the polarization degrees of freedom and the environment, the combined state may be written as $\hat{U}(\hat{\rho} \otimes \hat{\rho}_{\text{env}})\hat{U}^{\dagger}$. Averaging over the environmental degrees of freedom, which in our case are the different temporal modes of the photon itself, is equivalent to a partial trace of these degrees of freedom. Hence, the reduced polarization state can be written as

$$\hat{\rho}_f = \text{Tr}_{\text{env}}\{\hat{U}(\hat{\rho} \otimes \hat{\rho}_{\text{env}})\hat{U}^{\dagger}\}. \qquad (2)$$

Since the reduced polarization two-dimensional density matrix is obtained from a partial trace operation, it is useful to calculate only the diagonal terms that contribute to the final polarization state. The final state can be explicitly written as the sum of the $|\varphi\rangle$ amplitudes of the polarization states that occupy every temporal mode t:

$$\hat{\rho}_f = \sum_{t=1}^{T} |\varphi_t\rangle\langle\varphi_t|, \qquad (3)$$

where T is the number of all relevant temporal modes. Note that each $|\varphi_t\rangle$ is not normalized by itself. As a simple example for this calculation, we calculate the final polarization state for any initial pure state after passing through a single crystal. The initial polarization state is defined as

$$|\psi\rangle = \begin{pmatrix} \cos\left(\frac{\theta}{2}\right) \\ \sin\left(\frac{\theta}{2}\right)e^{i\phi} \end{pmatrix}, \qquad (4)$$

where the upper term corresponds to the $|h\rangle$ amplitude and the lower term corresponds to the $|v\rangle$ amplitude. Before applying every crystal of a scheme, the polarization basis should be rotated such that $|v\rangle$ is aligned along the crystal's fast axis. After the transmission through the crystal, the wave packet that occupies the $|v\rangle$ term exceeds the $|h\rangle$ wave packet by τ. Thus, the state can be written as

$$|\psi\rangle = \begin{pmatrix} \cos\left(\frac{\theta}{2}\right) \\ 0 \end{pmatrix}_{t=\tau} + \begin{pmatrix} 0 \\ \sin\left(\frac{\theta}{2}\right)e^{i\phi} \end{pmatrix}_{t=0}, \qquad (5)$$

and the reduced density matrix is therefore

$$\hat{\rho}_f = |\varphi_\tau\rangle\langle\varphi_\tau| + |\varphi_0\rangle\langle\varphi_0| = \begin{pmatrix} \cos^2\left(\frac{\theta}{2}\right) & 0 \\ 0 & \sin^2\left(\frac{\theta}{2}\right) \end{pmatrix}. \qquad (6)$$

The effect of wave plates is simple to calculate, as they rotate each of the temporal modes separately. From the resulting density matrix it is possible to calculate the DOP using Eq. (1).

With this method, it is possible to calculate the final polarization state for every initial arbitrary state that passes through a sequence of birefringent crystals-the depolarizer. For a specific depolarizing configuration, we define the channel

process $\mathcal{E}$ as the mapping of any arbitrary $\hat{\rho}$ to $\hat{\rho}_f = \mathcal{E}(\hat{\rho})$. This mapping can be uniquely described by the elements of the χ matrix [16]:

$$\mathcal{E}(\hat{\rho}) = \sum_{m,n} \chi_{mn} \hat{E}_m \hat{\rho} \hat{E}_n^\dagger, \qquad (7)$$

where $\hat{E}_m$ are matrices that span the space of $\hat{\rho}$ and χ is positive and Hermitian. It can be characterized by a QPT procedure which is composed of several quantum state tomography (QST) measurements of a set of a few initial $\hat{\rho}$ states.

III. EXPERIMENTAL RESULTS

In order to demonstrate the depolarizers' operation, we used the setup in Fig. 1. A 780-nm Ti:sapphire pulsed laser with 76-MHz repetition rate. It was frequency doubled, and the 390-nm pulses were focused into and collinearly down-converted in a 1-mm-thick type-I BaB$_2$O$_4$ (BBO) crystal. The down-converted signal was filtered by a dichroic mirror (DM) and collimated with a lens (L2). One photon of the pair was split by a beam splitter (BS) and detected, and the second photon was directed to the depolarizer. Actual rotation of the depolarizing crystals resulted with unwanted temporal and spatial walk-offs. Thus, we effectively rotated the crystals by rotating additional half-wave plates. The polarization state of the depolarized photons was characterized by wave plates and a polarizer (POL). Photons were filtered by 5-nm bandpass interference filters (IF), corresponding to a coherence time of $t_c \simeq 180$ fs, and then coupled into single-mode fibers leading to single photon detectors (DET). We characterized the depolarization of three initial states $|h\rangle$, $|p\rangle$, and $|r\rangle$, which are mutually unbiased [7], by QST [17]. The $|v\rangle$ state was also measured as required for QPT.

The first depolarizing scheme that we present is composed of two 2-mm-long calcite crystals C1 and C2 with two $\lambda/2$ wave plates (see Fig. 1). The crystals are fixed perpendicularly, with one wave plate before and the other after the first crystal. Rotation of the wave plates in opposite directions by an angle of $\theta/2$ is equivalent to the rotation of the first crystal by θ.

When $\theta = 0°$, no depolarization occurs, and when $\theta = 90°$, the depolarizer is equivalent to a dephasing channel of a single crystal.

The transformations of purely polarized states through the depolarizer for various angles between the two crystals are presented in Fig. 2. The measured output states for the three mutually unbiased states of $|h\rangle$, $|p\rangle$, and $|r\rangle$ are shown in Fig. 2(a), with a comparison to theory. We obtained all the measured states using a maximal-likelihood QST search [17] in order to avoid nonphysical final states (e.g., with $D > 1$) that can result when the depolarizer is tuned to almost no depolarization. The measured QPT mappings of the initial $D = 1$ sphere are shown for three specific cases in Figs. 2(b)–2(d). These cases are when the polarization of only one initial state is completely lost ($\theta = 45°$), when the channel is isotropic ($\theta = 54.7°$), and when two initial states are depolarized identically ($\theta = 67.5°$). A comparison between the measured and the theoretical χ matrices for $\theta = 54.7°$ is presented in Fig. 3. The channel fidelity was evaluated by applying the measured process to 700 initial states from the $D = 1$ surface of the Poincaré sphere. We calculated the theoretical output states for the same representative initial states, and the fidelities between the two output states were always higher than 97%.

The channel isotropy can be tested by comparing the final DOP of different input signals. The DOP results for the three input states of Fig. 2(a) are presented in Fig. 4 with their theoretical predictions. The three special cases of Figs. 2(b)–2(d) are clearly reproduced in our measurements. In general, this depolarizer is anisotropic, except for the special case of $\theta = 54.7° = \tan^{-1}(\sqrt{2})$. Analytical calculation of the DOP for this angle shows that the final value of $1/3$ is independent of the initial state, as can be seen in Fig. 4, where all three curves intersect, and in Fig. 2(c), where the polarization sphere is mapped to another sphere of radius $1/3$.

We studied a second depolarizing scheme that was composed of two perpendicularly fixed identical crystals with a quarter-wave plate between them (see Fig. 1). The quarter-wave-plate angle θ is set to be zero when the principal axes of
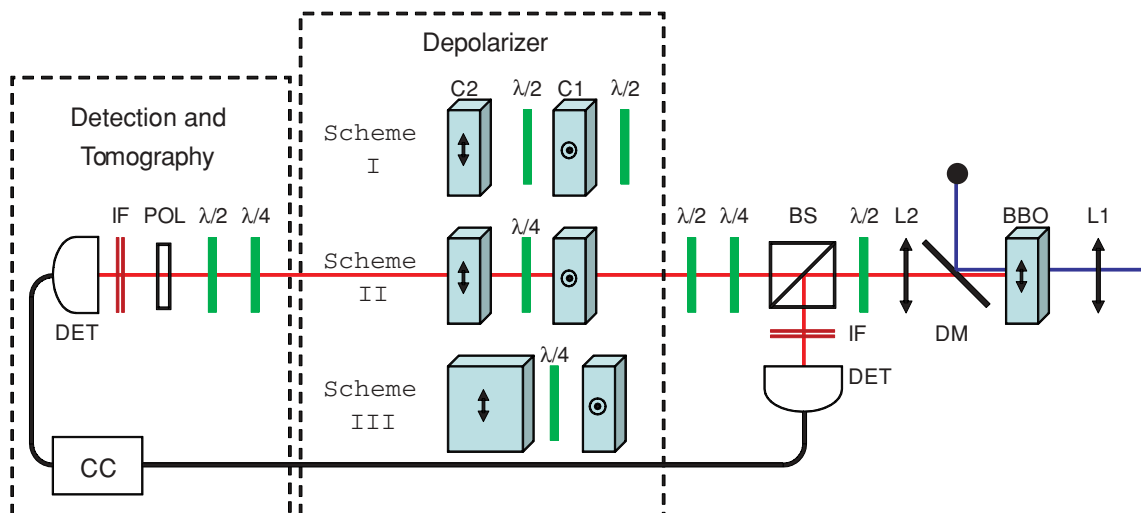

FIG. 1. (Color online) The experimental setup and depolarizing schemes. See full description in text.
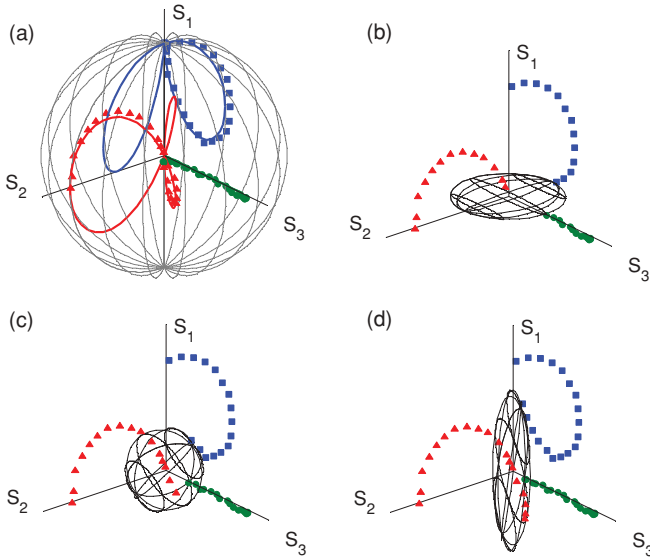
FIG. 2. (Color online) Experimentally measured final states and QPT in the Poincaré sphere representation for the first depolarizing scheme. (a) Comparison between measurements for $|h\rangle$ (blue squares), $|p\rangle$ (red triangles), and $|r\rangle$ (green circles) inputs in the range $0° < \theta < 90°$ and the theoretical model. Theoretical curves are presented as solid lines in the range $0° < \theta < 180°$. (b–d) Mapping of the surface of the Poincaré sphere to depolarized wire-mesh ellipsoids that was obtained by experimental QPT for the crystal angle values of (b) $\theta = 45°$, (c) $\theta = 54.74°$, and (d) $\theta = 67.5°$. Measured final states are plotted up to these angle values.

the wave plate and the first depolarizing crystal are parallel. For any given initial polarization $\{S_1, S_2, S_3\}$, the final DOP is

$$D^2 = \frac{1}{4}\left(\frac{19}{8} + \frac{3}{2}\cos(4\theta) + \frac{1}{8}\cos(8\theta)\right)$$
$$+ \frac{S_1^2}{4}\left(-\frac{7}{8} + \frac{1}{2}\cos(4\theta) + \frac{3}{8}\cos(8\theta)\right). \quad (8)$$

All states with the same $|S_1|$ value result in the same DOP for a certain θ. It is possible to find three mutually unbiased polarization bases that have the same $S_1 = \pm\frac{1}{\sqrt{3}}$ value and thus experience the same depolarization. We define this situation as symmetric depolarization. Notice that this is not an isotropic process. For such bases, the DOP can be tuned between 1 and $\frac{1}{\sqrt{6}} \approx 0.41$ as a function of θ. We generated such states
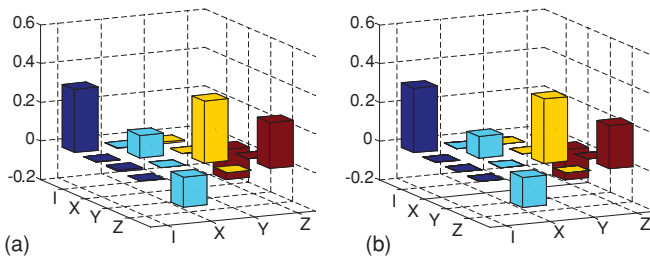

FIG. 3. (Color online) Real parts of the χ matrix that represents the isotropic process when $\theta = 54.74°$. (a) Measured matrix and (b) theoretically calculated matrix, both evaluated by a QPT procedure. The measured imaginary components are not presented, as they were relatively negligible, as expected.
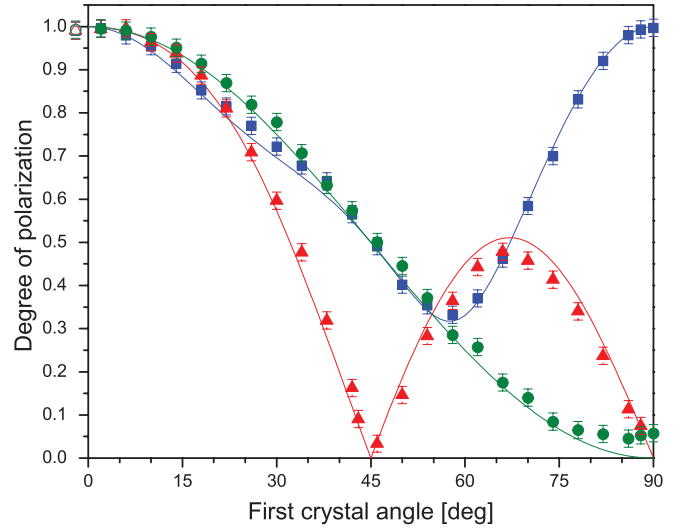

FIG. 4. (Color online) Experimentally measured degree of polarization of the output states as a function of the equivalent first-crystal rotation angle θ for the first depolarizing scheme. Initial states and their representations are the same as in Fig. 2. Model predictions are presented as solid lines. Errors are estimated according to the accuracy of the polarization optics.

and characterized them after passing them through the second depolarizing scheme. The generated mutually unbiased states were $\overline{S}_a = \{-\sqrt{1/3}, 0, \sqrt{1/2}\}$, $\overline{S}_b = \{-\sqrt{1/3}, \sqrt{1/2}, \sqrt{1/6}\}$, and $\overline{S}_c = \{-\sqrt{1/3}, -\sqrt{1/2}, \sqrt{1/6}\}$. Their DOP results as a function of θ are shown in Fig. 5(a), and their Poincaré representation is shown in Fig. 5(b). A good agreement with theory is observed.
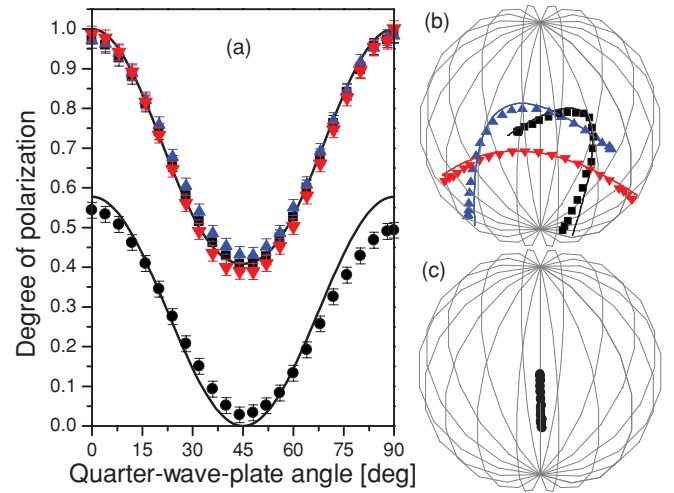

FIG. 5. (Color online) (a) Experimentally measured degree of polarization as a function of the quarter-wave-plate angle θ for the second and the third depolarizing schemes. For the second scheme, the three orthogonal initial states with $S_1 = -\sqrt{1/3}$ after depolarization are presented by black squares, blue triangles, and red inverted triangles. For the third scheme, the depolarized states of all three initial states should be identical. Results for one of these states are presented by black circles. (b, c) The measured states in the Poincaré sphere for the respective initial states.

REALIZING CONTROLLABLE DEPOLARIZATION IN . . .

PHYSICAL REVIEW A **83**, 022303 (2011)

The third scheme adds the possibility for symmetric depolarization down to complete depolarization. The difference between the second and third schemes is the doubling of the second crystal's thickness (see Fig. 1). As before, the final DOP depends only on the initial S_1 value and the wave-plate angle θ, but now it takes values between 0 and $\frac{1}{\sqrt{3}} \approx 0.58$. This result is due to an effective additional S_1 projection to the output of the second scheme. At the $\theta = 45°$ position, the third scheme is exactly a Lyot depolarizer that completely depolarizes any initial polarization by consecutive S_1 and S_3 projections.

Results for an initially polarized state with $S_1 = -\frac{1}{\sqrt{3}}$ are shown in Figs. 5(a) and 5(c). As can be seen, when $\theta = 45°$, the state is completely depolarized. The state tomography results [Fig. 5(c)] reveal the difference from the previous scheme as an extra S_1 projection.

IV. DISCUSSION

Although we have demonstrated the effects of the various depolarizing schemes using single photons, these depolarizers would also be effective on any classical light with sufficiently short coherence time. We repeated our measurements with laser pulses and demonstrated identical results (not presented here). Thus, these results apply not only to polarization encoded qubits but also to any classical scenario where controlled depolarization is required.

In this work, we use crystals that are long enough to completely separate the two polarization components. It is possible to deliberately use shorter crystals that will leave a portion of the two wave packets overlapping. The same qualitative results will be achieved this way but with smaller magnitude. It is possible also to use a combination of several concatenated schemes. This will extend the number of the temporal degrees of freedom and may result in better control of the isotropy level of the channel.

In many experiments, it is common to interfere two amplitudes of a single photon or the amplitude of two indistinguishable photons. We note that the effect of our depolarizers on such experiments has to be considered separately for each case. For example, the Hong, Ou, and Mandel bunching experiment [21] will not be altered by introducing the same depolarizers for both photons. On the other hand, although rotating one of the depolarizers by 90° does not change its depolarization, the two-photon interference will not be perfect anymore and will consist of several nonperfect bunching deeps.

V. CONCLUSIONS

We have demonstrated a scheme for the realization of various quantum channels for photon polarization qubits with controllable decoherence. Isotropic and anisotropic depolarization processes are possible. Channels were characterized by QPT using the maximal-likelihood algorithm. All the results are in a good agreement with a simple theoretical model. These depolarizers can be used to evaluate the performance of quantum error correction and quantum key distribution protocols. In addition, they can be utilized in any classical optics setup where controllable depolarization is required. The authors thank the Israeli Science Foundation for supporting this work under Grant No. 366/06.

[1] G. G. Stokes, Trans. Cambridge Philos. Soc. **9**, 399 (1852).

[2] N. Hodgson and H. Weber, *Laser Resonators and Beam Propagation: Fundamentals, Advanced Concepts, and Applications*, 2nd ed. (Springer, Berlin, 2005), pp. 171–172.

[3] B. Lyot, Ann. Obser. Paris **8**, 102 (1929).

[4] A. P. Loeber, J. Opt. Soc. Am. **72**, 650 (1982).

[5] M. A. Nielsen and I. L. Chuang, *Quantum Computation and Quantum Information* (Cambridge University Press, Cambridge, UK, 2000).

[6] C. H. Bennett and G. Brassard, *Proceedings of the IEEE International Conference on Computers, Systems, and Signal Processing, Bangalore, India* (IEEE, New York, 1984), p. 175.

[7] D. Bruß, Phys. Rev. Lett. **81**, 3018 (1998).

[8] P. G. Kwiat, A. J. Berglund, J. B. Altepeter, and A. G. White, Science **290**, 498 (2000).

[9] G. Puentes, A. Aiello, D. Voigt, and J. P. Woerdman, Phys. Rev. A **75**, 032319 (2007).

[10] S. P. Morgan, M. P. Khong, and M. G. Somekh, Appl. Opt. **36**, 1560 (1997).

[11] G. Puentes, D. Voigt, A. Aiello, and J. P. Woerdman, Opt. Lett. **30**, 3216 (2005).

[12] B. H. Billings, J. Opt. Soc. Am. **41**, 966 (1951).

[13] M. Karpiński, C. Radzewicz, and K. Banaszek, J. Opt. Soc. Am. B **25**, 668 (2008).

[14] Y. Nambu *et al.*, Proc. SPIE Int. Soc. Opt. Eng. **4917**, 13 (2002).

[15] G. Puentes, D. Voigt, A. Aiello, and J. P. Woerdman, Opt. Lett. **31**, 2057 (2006).

[16] I. L. Chuang and M. A. Nielsen, J. Mod. Opt. **44**, 2455 (1997).

[17] J. B. Altepeter, E. R. Jeffrey, and P. G. Kwiat, Adv. At. Mol. Opt. Phys. **52**, 105 (2005).

[18] A. Al-Qasimi, O. Korotkova, D. James, and E. Wolf, Opt. Lett. **32**, 1015 (2007).

[19] S. Lu and A. P. Loeber, J. Opt. Soc. Am. **65**, 248 (1975).

[20] O. Kern and J. M. Renes, Quant. Inf. Comput. **8**, 756 (2008).

[21] C. K. Hong, Z. Y. Ou, and L. Mandel, Phys. Rev. Lett. **59**, 2044 (1987).

022303-5